

## **BASIS OF IONOSPHERIC MODIFICATION BY HIGH-FREQUENCY WAVES**

**S. P. Kuo**

Department of Electrical and Computer Engineering  
Polytechnic University  
6 MetroTech Center, Brooklyn, NY 11201, USA

**Abstract**—The requirements of achieving ionospheric modification by ground-transmitted HF heating waves are discussed. The directly relevant processes including linear mode conversion and parametric instabilities are explained physically. The nonlinear Schrodinger equation for Langmuir waves is reviewed and the initial conditions of two types of nonlinear solutions are discussed; from which the criterion for Langmuir soliton generation is pointed out.

### **1. INTRODUCTION**

Ionospheric heating and modification by powerful HF waves transmitted from the ground has been a very active research area over the past three decades [1–3]. It is an ideal approach for experimental and theoretical investigation of the linear and nonlinear properties of the ionospheric plasma. Through the observations of many unexpected phenomena [3, 4], considerable progress toward the understanding of the nonlinear plasma processes has been accomplished. A major facility for conducting ionospheric heating experiments in Gakona, Alaska, as part of the High Frequency Active Auroral Research Program (HAARP) [5], is being upgraded. The upgraded HAARP HF transmitting system will be a phased-array antenna of 180 elements. Each element is a cross dipole, which radiates a circularly polarized wave up to 20 kW in the frequency band from 3 MHz to 10 MHz. The antenna gain, which increases with the radiating frequency, varies from 15 dB to 30 dB. Thus an effective radiated power (ERP) of 90 dBW will be available in heating experiments, which explore modification effects on the bottom-side of the ionosphere as illustrated in Fig. 1.

Electromagnetic waves interact with charged particles in the ionosphere and only electrons can effectively respond to the fast

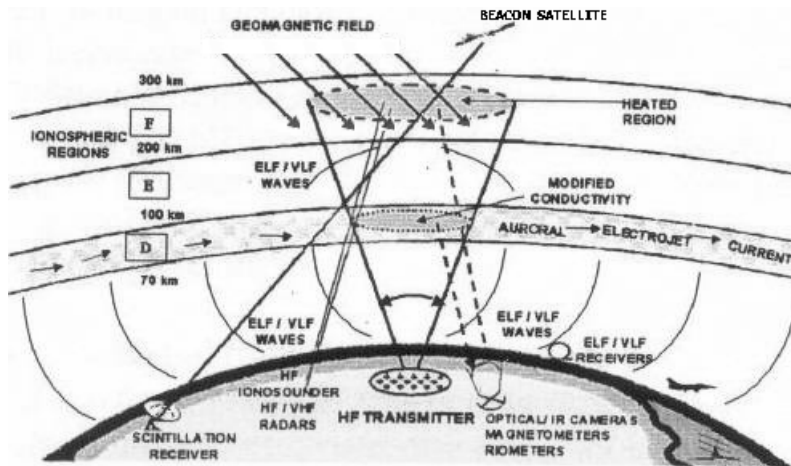


**Figure 1.** Ionospheric heating experiments and some remote sensing facilities.

oscillations of HF waves. Neutral particles can also experience the presence of HF waves through elastic and inelastic collisions with charged particles (mainly electrons). In *D* and *E* regions, the density of neutral particles is high, which results in a higher electron-neutral collision frequency than electron-electron and electron-ion collision frequencies. Therefore, in those regions, neutral particles can share a considerable percentage of wave energy with plasma. Neutral particles thermalize the indirectly absorbed wave energy rapidly; but neutral particles have much higher density that reduces the energy share of each one and thus limits their temperature increase. Consequently, the HF modification in those regions is not expected to be effective, except that the electrojet current appearing in these regions can be modulated by intensity modulated HF heating to become a virtual antenna, which radiates ELF/VLF waves for underwater communications [6]. Therefore, in most HF heating experiments the focus is on the *F* region modification, where the wave energy delivered to the plasma is mainly distributed in electrons, and non-thermal processes may prevail because the energy thermalization and temperature equilibrium time are much longer. Indeed, many nonlinear plasma processes occurring in this region have been observed in the heating experiments.

However, the collision (electron-electron and electron-ion) process will not be effective enough to absorb the electromagnetic (EM) wave energy delivered to the *F* region of the ionosphere. Preparations of heating waves in experiments are necessary in order to effectively trap

the wave energy there and thus to optimize the HF modification effects on the ionosphere. First, the frequency of the heating wave is chosen to be below the maximum cutoff frequency of the ionosphere to keep the wave energy in the bottom-side region. However, the heating wave may be reflected back to the ground. To avoid this, a fast conversion of the EM heating wave into electrostatic (ES) waves of the plasma is necessary. This is because ES waves are supported by the plasma and only stay in the plasma. Then the question is how to convert an EM wave into ES waves. In general, there are two processes: linear and nonlinear mode conversion processes.

Before discussing mode conversion, a comment on the wave features is in order. In general, a wave is characterized by its frequency and wavelength. In the plasma, a wave is also characterized by its polarization, which refers to the direction of the wave electric field (rather than that of the magnetic field). Using the wave propagation direction as a reference direction, there are three types of waves, in terms of their polarizations, that exist in plasma: transverse (EM), longitudinal (ES), and hybrid. Transverse means that the wave electric field is perpendicular (transverse) to the wave propagation direction; hence, a transverse wave is an EM wave that also carries magnetic field. Longitudinal means that the wave electric field is parallel to the propagation direction; in essence, it is an ES wave because no magnetic field is induced by the wave electric field. Plasma becomes anisotropic when a dc magnetic field is imposed; the wave electric field may have an angle other than  $0^\circ$  or  $90^\circ$  with respect to the propagation direction (i.e., a combination of EM and ES polarization). In this situation, the wave is a hybrid mode type.

## 2. MODE CONVERSION

A mode of a system is an oscillation that can self-sustain in the system. For example, apply an impulse to a (lossless) system; oscillations at all frequencies will be excited. However, not all the oscillations can persist in time; in fact, most of the oscillations will be damped away via phase mixing (among themselves or caused by the boundary effects). In the steady state, only a few oscillations may stay, and these lasting oscillations are the “modes” of the system. In a lossless system, the modes are “eigen-modes”. In practice, there are always some losses in the system; in this case, modes are also damped in time (but much slower) and are “quasi-modes”. In the mathematical analysis, modes represent the source-free solutions of the system’s governing equations. Therefore,  $(\omega-k)$  relations are determined by requiring the solutions of the source-free equations to be nontrivial (i.e., non-zero solutions).

These relations are called dispersion relations, which may be plotted on a  $k$ - $\omega$  plane as dispersion curves. Each curve represents a mode branch and each point on the curve is a mode of the system.

Linear mode conversion may occur in the ionosphere because it is inhomogeneous magneto plasma. Magneto plasma supports various branches of plasma modes, which are EM, ES, or hybrid mode type depending on the frequency regime, polarization, and the propagation angle with respect to the geomagnetic field. As explained in the preceding paragraph, a dispersion relation represents a plasma mode branch and is a functional dependence of the wave frequency  $\omega$  on the propagation constant  $k$ . Since magneto plasma is an anisotropic (uniaxial) medium,  $\omega$  is a function of  $k_{\parallel}$  and  $k_{\perp}$ , where the subscripts  $\parallel$  and  $\perp$  stand for components parallel and perpendicular to the magnetic field; thus the dispersion curves (i.e.,  $\omega$ - $\mathbf{k}$  relations) of magneto plasma should be plotted in three-dimensional spectral space ( $k_{\parallel}, k_{\perp}, \omega$ ). However, a three-dimensional diagram is not convenient for explaining the physical phenomena to be discussed later. Therefore, a conventional way is to only plot the dispersion curves for the  $0^{\circ}$  and  $90^{\circ}$  propagation cases; in these special cases,  $\omega$  is a function of  $|\mathbf{k}|$  ( $= k$ ). Thus these curves can be combined together in a single two-dimensional diagram on the  $k$ - $\omega$  plane such as the one exemplified in Fig. 2 (for downward magnetic field and cold plasma). In this figure, only high frequency branches relevant to the following discussion are plotted and the cutoff frequencies  $\omega_1$  (for the  $L$  and  $X$  branches) and  $\omega_2$  (for the  $R$  branch) and upper hybrid resonance frequency  $\omega_u$  are also expressed. Hence, a branch for an arbitrary propagation angle can be located in the region between a pair of  $0^{\circ}$  and  $90^{\circ}$  branches.  $k_{\parallel}$  in the plot represents the component, parallel to the geomagnetic field, of the wavevector. Among the curves in Fig. 2,  $L$  and  $X$  is a pair to confine the region of the  $X$ -mode branch for the propagation angle from  $0^{\circ}$  to  $90^{\circ}$ . Likewise,  $R$  and  $O$  pair for the  $O$ -mode branch. The polarization of the incident heating wave determines its mode type. A left-hand (LH) circularly polarized wave falls into the  $X$ -mode branch, and the  $O$ -mode branch starts with incident wave of right-hand (RH) circular polarization. It is noted that Fig. 2 is plotted for uniform plasma, i.e., for constant plasma frequency  $\omega_P$  and electron cyclotron frequency  $\Omega_e$ . However, the ionosphere is not uniform; although  $\Omega_e$  may be considered to be a constant at each heating site,  $\omega_P$  increases with the altitude in the bottom-side of the ionosphere. As a HF heater of a fixed frequency  $\omega_0$  propagates upward,  $\omega_P$  in Fig. 2 moves upward along the vertical ( $\omega$ ) axis. Consequently, all the dispersion curves will also move upward accordingly. This will be inconvenient in describing wave propagation because Fig. 2 has to be modified constantly. However, there is a way to

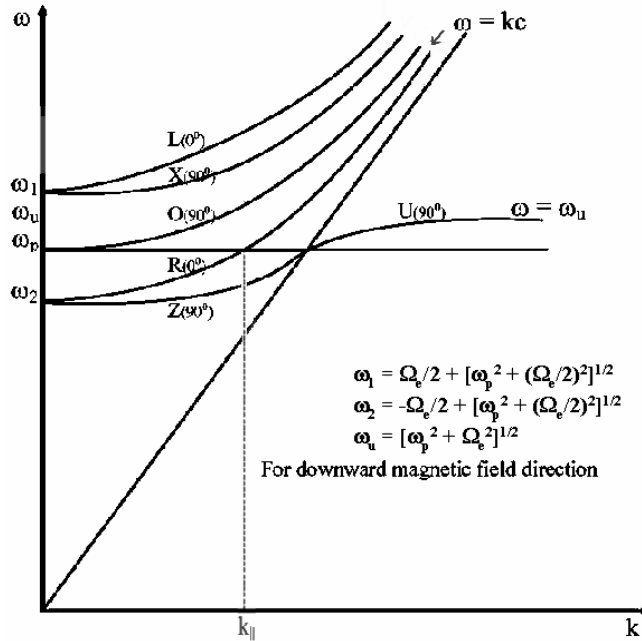


**Figure 2.** Dispersion curves of high frequency EM waves propagating along (0°) and perpendicular (90°) to the geomagnetic field.

fix  $\omega_P$  on the vertical axis of Fig. 2: by constantly rescaling the  $\omega$  axis during the wave propagation. For example, as the wave propagates upward, the scale of the  $\omega$  axis is increased accordingly to keep  $\omega_P$  at the same point on the axis. Consequently,  $\omega_0$  of the wave has to move down along the  $\omega$  axis. In other words, the dispersion curves in Fig. 2 will remain unchanged as the wave propagates upward; but the point on an appropriate dispersion curve to represent the propagating wave mode will move downward along this dispersion curve (which is between a pair of 0° and 90° curves). A more precise way to follow the wave trajectory is to employ a ray tracing technique [7].

### 2.1. Linear Mode Conversion

Linear mode conversion may occur at the point of intersection of two mode branches. As shown in Fig. 2, the *O*-mode and *R*-mode branches intersect with the electron plasma mode branch. Thus the HF heating wave is set with RH circular polarization and Fig. 2 will be used in the discussion of linear mode conversion. Consider a RH circularly polarized wave propagating upward, with an arbitrarily

inclined angle  $\theta_0$ , into the ionosphere as indicated by the arrow in Fig. 2; the vertically upward component of the wavevector, having the initial magnitude  $k_0 \cos \theta_0$ , will decrease continuously as the plasma density increases continuously, where  $k_0 = \omega_0/c$  and  $\omega_0$  is the wave frequency. Consequently, the angle of inclination of the wave, with respect to the geomagnetic field, also changes continuously. When the wave reaches near the  $O$ -mode reflection height indicated by the horizontal line  $\omega = \omega_p$ , the wave will turn toward either 1) the  $O$ -curve or 2) the  $R$ -curve, depending on the initial angle of inclination (related to the injection angle). In either case, the wave will reach an intersecting point on the  $\omega = \omega_p$  line. In the first situation, for example, for a vertically incident wave ( $\theta_0 = 0$ ), the wave propagation direction turns toward perpendicular to the geomagnetic field (with the wavevector  $\mathbf{k} \rightarrow 0$ ). The intersecting point located at ( $k = 0, \omega_0 = \omega_p$ ) is a cutoff point, where the wave experiences reflection; and in the nearby region the polarization of the wave is drastically different from that of the electron plasma wave (i.e., Langmuir wave), which has a preferred direction parallel to the geomagnetic field. Therefore, the linear mode conversion to directly convert the heating wave to the Langmuir wave will not occur.

The second situation, where the wave turns to follow the  $R$ -curve requires a proper injection angle of the heating wave. In this case, the wave at the point of intersection ( $k = k_{\parallel}, \omega_0 = \omega_p$ ) does not experience total reflection. Instead, the wave tends to continuously propagate upward along the geomagnetic field to become a  $Z$ -mode in the region above the  $O$ -mode reflection height. However, this linear mode conversion can occur effectively if the wave at the intersecting point can satisfy a phase matching condition, which requires  $\theta_0 = \theta_s$ , the Spitz angle, to be elaborated with the aid of Fig. 3.

Since the ionospheric plasma density is horizontally stratified, the horizontal component ( $k_0 \sin \theta_s$  in Fig. 3) of the wave vector is conserved in the propagation. Thus the horizontal component of the wavevector at the intersecting point,  $k_{\parallel} \sin \alpha$ , should equal to  $k_0 \sin \theta_s$ . If the wave converts to a  $Z$ -mode, ( $k_{\parallel}, \omega_0$ ) have to satisfy the  $R$ -wave dispersion relation:  $1 - \omega_p^2/\omega(\omega + \Omega_e) = (kc/\omega)^2$ , under the condition  $\omega_0 = \omega_p$ . Thus the phase matching condition to convert the incident wave to a  $Z$ -mode is given by  $k_0 \sin \theta_s = k_{\parallel} \sin \alpha$ , where  $k_{\parallel} = k_0[\Omega_e/(\omega_0 + \Omega_e)]^{1/2}$  determined by the  $R$ -wave dispersion relation. The Spitz angle is then determined to be

$$\theta_s = \sin^{-1}\{[\Omega_e/(\omega_0 + \Omega_e)]^{1/2} \sin \alpha\}$$

After the reflection of the  $Z$ -mode at its reflection height  $\omega_{pZ} = [\omega_0(\omega_0 + \Omega_e)]^{1/2}$ , this wave propagates downward to the region near

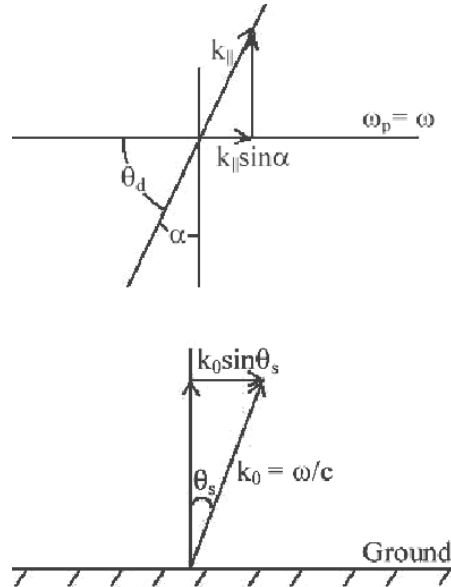


**Figure 3.** Phase matching condition for mode conversion.

the upper hybrid resonance layer at  $\omega_{pU} = (\omega_0^2 - \Omega_e^2)^{1/2}$  to become an upper hybrid wave. Therefore, through this linear mode conversion, the heating wave energy will be trapped in the region between the  $\omega_p = \omega_{pZ}$  and  $\omega_{pU}$  layers.

### 2.2. Nonlinear Mode Conversion

Another effective way (and probably the most effective way) to convert the HF heating wave to plasma waves is through parametric instabilities, by which the heater decays into a high frequency electron wave and a low frequency ion wave. Such a decay process involves mode-mode couplings through the nonlinearity of plasma; hence it is termed nonlinear mode conversion. Because the decay process preferred the decay waves (in particular, the high frequency electron mode) to be plasma modes to minimize the instability threshold condition, the heating wave has to be accessible to the regions, where the high frequency plasma mode frequencies are close to the heating wave frequency. As shown in Fig. 2, the LH circularly polarized wave will be reflected at a height  $\omega_{px} = [\omega_0(\omega_0 - \Omega_e)]^{1/2}$  that is below the electron plasma resonance layer  $\omega_{pO} = \omega_0$  as well as the upper hybrid resonance layer  $\omega_{pU} = (\omega_0^2 - \Omega_e^2)^{1/2}$ . Therefore, in *F*-region

modification experiments, only RH circularly polarized heating waves are used. Heating waves then converted to the  $O$ -mode (if the incident angle does not closely match the Spitzer angle) in the region near the HF reflection height, which is located above the upper hybrid resonance layer and overlaps with that of the electron plasma resonance layer. Therefore, the heating wave is accessible to the spatial regions, where many parametric coupling conditions can be matched. Moreover, the heating wave electric field is enhanced by a “swelling effect” near its reflection height. This makes it easy to excite instabilities, which have threshold field requirements, and also works to increase the growth rates of the instabilities. The swelling effect will be described in detail in Section 4.

### 3. PARAMETRIC INSTABILITIES

A parametric amplifier uses three coupled resonant circuits (e.g., LC circuits) to convert frequency from one to another. A nonlinear (variac) capacitor  $C$  in the circuit provides the coupling (i.e., frequency mixing). The three resonant modes, oscillating at  $\omega_0, \omega_1$ , and  $\omega_S$ , in a parametric amplifier are called the source (pump), idler (sideband), and signal (decay mode), where the frequency matching condition  $\omega_0 = \omega_1 + \omega_S$  is satisfied. Generalize the basic principle for wave amplification in a circuit to a system: one recognizes that the system has to be able to support at least three branches of modes and carries nonlinear properties to provide mechanisms for wave-wave couplings.

Plasma can support high frequency EM waves, as well as electrostatic (ES) plasma waves of high and low frequencies as plasma modes that oscillate in plasma as thermal fluctuations in the absence of external sources. In essence, plasma is a nonlinear medium. Therefore, parametric coupling among three modes can occur. When a large amplitude high frequency wave  $\mathbf{E}_p(\omega_0, \mathbf{k}_p)$  (either EM or ES) appears in plasma, this wave can act as a pump wave to excite plasma modes through parametric couplings. For example, this pump wave electric field can drive a nonlinear current in the electron density perturbation  $n_s(\omega_s, \mathbf{k}_s)$  of a low frequency plasma mode to produce beat waves  $\mathbf{E}_1(\omega_1, \mathbf{k}_1)$  and  $\mathbf{E}'_1(\omega'_1, \mathbf{k}'_1)$ . Since these are propagating waves, their wavevectors, in addition to the frequencies, also have to be matched in the couplings. In other words, both frequency and wavevector matching conditions:

$$\omega_0 = \omega_1 + \omega_s^* = \omega'_1 - \omega_s \quad \text{and} \quad \mathbf{k}_p = \mathbf{k}_1 + \mathbf{k}_s = \mathbf{k}'_1 - \mathbf{k}_s$$

are imposed in parametric couplings in plasmas. The strength of the coupling depends on the involved nonlinearities and the nature of the

induced beat wave. The coupling is strong when

the beat wave is resonant with plasma (i.e., a plasma mode). Beat waves, in turn, also couple with the pump wave to introduce a low frequency nonlinear force on electrons, which produces plasma density perturbation having the same frequency and wavevector as  $n_s(\omega_s, \mathbf{k}_s)$ . Hence, this coupling produces a feedback to the original density perturbation  $n_s(\omega_s, \mathbf{k}_s)$ . If the feedback is positive and large enough to overcome linear losses of coupled waves, the coupling becomes unstable and coupled waves grow exponentially at the expense of pump wave energy. This is called “parametric instability”, by which the pump wave  $\mathbf{E}_p(\omega_0, \mathbf{k}_p)$  decays to two sidebands  $\mathbf{E}_1(\omega_1, \mathbf{k}_1)$  and  $\mathbf{E}'_1(\omega'_1, \mathbf{k}'_1)$  through a low frequency decay mode  $n_s(\omega_s, \mathbf{k}_s)$ . This instability process involves the nonlinearity of the plasma and thus is a nonlinear instability. The parametric coupling is imposed by the frequency and wavevector matching conditions as well as a threshold condition on the pump wave field intensity.

This process can be reduced to a three-wave coupling process when the decay mode  $n_s(\omega_s, \mathbf{k}_s)$  has a finite oscillating frequency. In this situation, two sidebands cannot satisfy the same dispersion relation simultaneously. Thus the frequency-upshifted sideband  $\mathbf{E}'_1(\omega'_1, \mathbf{k}'_1)$  is off resonant with plasma and can be neglected in the coupling.

The most effective parametric instabilities excited directly by the electromagnetic heating wave are 1) Parametric decay instability (PDI) and 2) Oscillating two-stream instability (OTSI), in both mid-latitude and high-latitude regions [4, 8, 9]. The sidebands in the mid-latitude region are Langmuir waves. In the high-latitude region, the sidebands can be upper hybrid waves or Langmuir waves. However, the instabilities involving the Langmuir waves as sidebands have to compete with those excited in the lower altitudes and having upper hybrid waves as sidebands. Dipole pump, i.e., its wavevector  $\mathbf{k}_0 = 0$ , can be assumed. This is because these instabilities are excited in the region near the  $O$ -mode reflection height and the sidebands and decay mode are electrostatic waves, which have much larger wavenumbers.

### 3.1. Parametric Decay Instability (PDI)

This is a three-wave coupling process represented by

$$\text{EM Pump } (\omega_0, \mathbf{k}_0 = 0) \rightarrow (\omega_1, \mathbf{k}_1) + (\omega_s^*, \mathbf{k}_s)$$

where  $\mathbf{k}_s = -\mathbf{k}_1$ ;  $(\omega_1, \mathbf{k}_1)$  and  $(\omega_s, \mathbf{k}_s)$  are Langmuir sideband and ion acoustic wave.

### 3.2. Oscillating Two Stream Instability (OTSI)

This is a four-wave coupling process represented

$$\text{EM Pump } (\omega_0, 0) \rightarrow \begin{cases} (\omega_1, \mathbf{k}_1) + (-i\gamma, \mathbf{k}_s) \\ (\omega_1, -\mathbf{k}_1) - (i\gamma, \mathbf{k}_s) \end{cases}$$

where again  $\mathbf{k}_s = -\mathbf{k}_1$ ;  $(\omega_1, \pm\mathbf{k}_1)$  and  $(i\gamma, \mathbf{k}_s)$  are Langmuir sidebands and purely growing mode.

PDI and OTSI having the upper hybrid wave as a sideband have similar representations. The instability processes usually prefer the excited waves to be plasma modes. The instability threshold can increase considerably if the  $\omega$ - $\mathbf{k}$  relationships of the excited waves are too far from the dispersion relations of the plasma modes. For example, the threshold of OTSI is higher than that of PDI because a purely growing mode is not a plasma mode and the sidebands are also slightly off from the Langmuir mode.

In heating experiments, the wavenumbers of HF enhanced plasma lines and ion lines (HFPLs and HFILs) are fixed by the wavenumber of backscatter radar. Thus the HFPLs and HFILs contributed by PDI and OTSI originate from narrow regions below the O-mode reflection height, where the electron plasma frequency  $\omega_P = \omega_0$ .

### 3.3. HFPLs

In general, HF heating waves produce an abundance of wave phenomena through parametric instabilities. However, remote sensing by radars cannot explore all of them. For example, backscatter radars cannot detect upper hybrid waves, whose excitation by the HF heating waves in high-latitude region is inferred by the ground measurements on stimulated electromagnetic emissions (SEEs). Radar detection is based on incoherent and coherent scatterings from the target. In probing background plasma, return signals come from incoherent scatterings. On the other hand, plasma waves can scatter radar signal coherently with much larger scattering cross sections, which make the return signals have large signal to noise ratios. The coherent scattering satisfies the Bragg scattering condition, i.e., the frequencies and wavevectors of the scattered waves  $(\omega_{B\mp}, \mathbf{k}_{B\mp})$ , plasma waves  $(\omega_L, \mathbf{k}_L)$ , and incident radar wave  $(\omega_R, \mathbf{k}_R)$  are related by the relations  $\omega_{B\mp} = \omega_R \mp \omega_L$  and  $\mathbf{k}_{B\mp} = \mathbf{k}_R \mp \mathbf{k}_L$ . In general,  $\omega_R \gg \omega_L$ ; thus  $|\mathbf{k}_{B\mp}| \cong |\mathbf{k}_R| = \omega_R/c$ . Therefore, in the backscattering case,  $\mathbf{k}_{B\mp} \cong -\mathbf{k}_R$  and  $\mathbf{k}_L \cong \pm 2\mathbf{k}_R$ . In other words, radar can only effectively detect those Langmuir waves having wavenumbers twice the wavenumber of the probing radar signal and propagating parallel (up-going) or anti-parallel (down-going) to the pointing direction of the

radar. These recorded spectral lines are termed “HF enhanced plasma lines (HFPLs)”. The up-going plasma wave scatters the radar signal to produce a frequency-downshifted radar return  $(\omega_{B-}, \mathbf{k}_{B-})$ , and the frequency-upshifted radar return  $(\omega_{B+}, \mathbf{k}_{B+})$  is produced by scattering the radar wave over the down-going plasma wave. In general, the spectrogram of HFPLs records the spectrum of the radar return signals at frequencies offset by  $\omega_R \mp \omega_0$ . Therefore, the spectral lines of up-going plasma waves will appear in the spectrogram as cascading to the right hand side (positive frequency side) with increasing frequencies. On the other hand, the spectral lines of down-going plasma waves will appear in the spectrogram as cascading to the left hand side (negative frequency side) with decreasing frequencies.

### 3.4. Langmuir Cascade

Langmuir waves excited by OTSI and PDI in the region below the HF reflection height can become pump waves to excite new parametric instabilities, which generate frequency-downshifted Langmuir waves to be their sidebands. This is called “Langmuir cascade”. Continuous cascade of Langmuir waves through new parametric instabilities broadens the downshifted frequency spectrum of Langmuir waves [10, 11]. A similar description is also applicable to the “upper hybrid cascade”. The permissible number of cascade and the required pump threshold field vary with each cascade process that can be distinguished by the nature of the low frequency decay mode. In the following, a Langmuir cascade process that involves an ion acoustic wave as the decay mode is discussed. This three-wave coupling process is represented by

$$\text{Langmuir Pump } (\omega_1, \mathbf{k}_1) \rightarrow (\omega_2, \mathbf{k}_2) + (\omega_s^*, \mathbf{k}_s)$$

where  $\mathbf{k}_s = \mathbf{k}_1 - \mathbf{k}_2 \cong 2\mathbf{k}_1$ ;  $(\omega_2, \mathbf{k}_2)$  and  $(\omega_s, \mathbf{k}_s)$  are Langmuir sideband and ion acoustic wave.

How the frequency and wavevector matching conditions of the parametric coupling processes can be satisfied through the coupled plasma waves is illustrated in Fig. 4, which exemplifies this Langmuir cascade process with the special situation that  $\mathbf{k}_1, \mathbf{k}_2$ , and  $\mathbf{k}_s$  are parallel to the geomagnetic field to simplify the plot. In the figure, the dispersion curves of the Langmuir wave (represented by the parabola, which asymptotically approaches the line labeled  $\omega = kv_{te}$  and its mirror image) and the ion acoustic wave (represented by the straight line labeled  $\omega = kC_S$  and its mirror image) are plotted on the  $\omega$ - $k$  plane. Thus each wave (or mode) labeled by its frequency and wavenumber  $(\omega, k)$  can be represented by a position vector of the

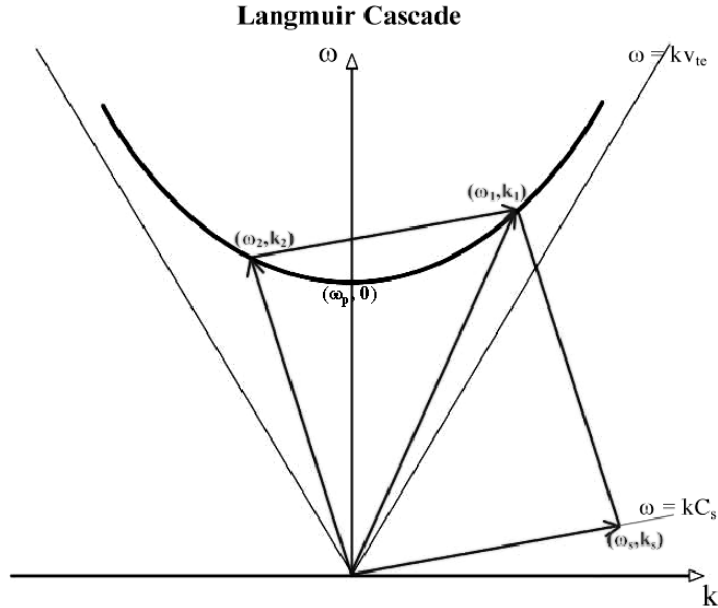


**Figure 4.** Vector relations showing the frequency and wavevector matching arrangements on the dispersion plane to identify the plasma modes in the parametric coupling.

corresponding point on the plane. In this representation, the frequency and wavenumber matching conditions are combined into a single vector matching condition.

Starting at a point  $(\omega_1, \mathbf{k}_1)$  on the right-hand side (RHS) of the parabola, which represents a Langmuir wave excited by PDI, a downward inclined line parallel to the line  $\omega = kC_S$  is drawn to intersect with the parabola. The intersecting point  $(\omega_2, \mathbf{k}_2)$  on the left-hand side (LHS) of the parabola determines the sideband. The vector between the two points  $(\omega_1, \mathbf{k}_1)$  and  $(\omega_2, \mathbf{k}_2)$  can then be mapped on the  $\omega = kC_S$  line to identify the decay mode. The matching conditions are satisfied as indicated by the vector relations shown in the figure. A similar procedure starting at the point  $(\omega_2, \mathbf{k}_2)$  can be applied to determine the plasma modes  $(\omega_3, \mathbf{k}_3)$  in the subsequent cascade. However, one can easily find that  $|k_3|$  will be smaller than  $|k_2|$  (likewise,  $|k_2| < |k_1|$ ). On the other hand, HFPLs have a fixed  $k$  value. Therefore, the parabola has to move down slightly in each subsequent cascade to keep the sideband to have a fixed  $|k|$ . In other words, the cascade lines in the HFPLs contributed by this cascade process originate from a relatively thick layer. In the frequency spectrum of HFPLs, the first

spectral peak having the highest frequency at  $\omega = \omega_1$  is an OTSI line if  $\omega_1 = \omega_0$ , the heating wave frequency; if  $\omega_1$  is downshifted from  $\omega_0$  by  $\Delta\omega = \omega_0 - \omega_1 = \omega_{S0} = 2k_R C_s$ , where  $k_R$  is the wavenumber of the probing backscatter radar signal, then it is a PDI line; the subsequent spectral peaks at  $\omega_2, \omega_3, \dots$  correspond to the first, second,  $\dots$  cascade lines. The cascade lines are recognized by doubling their frequency downshift from the preceding line to  $2\omega_{S0}$ .

For example, if a spectrogram of HFPLs contains 7 spectral peaks starting at  $\omega = \omega_0$ , then the first two spectral peaks at  $\omega = \omega_0$  and  $\omega_0 - \omega_{S0}$  are called OTSI and PDI lines, respectively. The remaining 5 spectral peaks at  $\omega_0 - (2n + 1)\omega_{S0}$ ,  $n = 1, \dots, 5$  are called cascade lines and their first pump is a sideband of the PDI. In this case, the spectral width of HFPLs is about  $11\omega_{S0}$ .

#### 4. WAVE PROPAGATION IN A NON-UNIFORM MEDIUM

Propagation of a heating wave is governed by the Helmholtz equation

$$d^2 E/dz^2 + k^2(z)E = 0 \quad (1)$$

where  $k^2(z) = [\omega_0^2 - \omega_p^2(z)]/c^2$ ,  $\omega_0$  is the wave frequency,  $\omega_p(z) = [4\pi n_e(z)e^2/m_e]^{1/2}$  is the electron plasma frequency, and the electron density  $n_e(z)$  increases with the altitude; geomagnetic field is not included in the formulation to simplify the analysis and presentation. Therefore,  $k(z)$  decreases as wave propagates upward. Consider the situation that  $\omega_0$  is less than the plasma frequency at the  $F$ -peak of the ionosphere (where the plasma density is the maximum). In that case, the wave can reach a layer at  $z = z_0$ , where  $\omega_p(z_0) = \omega_0$  and  $k(z_0) = 0$ . This point  $z_0$  is called the turning point, where wave reflection occurs. If the wave is not near a turning point (i.e., reflection point)  $z_0$ , the WKB solution [12]  $E = A_0(k)^{-1/2} \exp[\pm i \int^z k(z) dz]$  of (1) is a good approximation.

##### 4.1. Solution of the Wave Equation near a Turning Point

In the vicinity of  $k \rightarrow 0$ , the electron density can be assumed to have a linearly increasing profile, i.e.,  $n_e(z) = n_0[1 + (z - z_0)/L]$ , where  $n_0 = n_e(z_0)$  and  $L$  is the linear scale length. Hence,  $\omega_p^2(z) = \omega_0^2[1 + (z - z_0)/L]$ , and  $k^2(z) = [\omega_0^2 - \omega_p^2(z)]/c^2 = \nu(z_0 - z)$ , where  $\nu = \omega_0^2/Lc^2$ . Moreover, if a new coordinate  $g = z_0 - z$  is introduced, then (1) becomes

$$d^2 E/dg^2 + \nu g E = 0 \quad (2)$$

A coordinate transformation,  $y = (2/3)(\nu g^3)^{1/2}$ , leads to  $d/dg \rightarrow \nu^{1/2}(3/2\nu^{1/2})^{1/3}y^{1/3}d/dy$  and  $d^2/dg^2 \rightarrow \nu(3/2\nu^{1/2})^{2/3}y^{2/3}d^2/dy^2 + (\nu^{1/2}/2)(2\nu^{1/2}/3)^{1/3}y^{-1/3}d/dy$ ; and letting  $E = g^{1/2} F$ , i.e.,  $E = (3/2\nu^{1/2})^{1/3}y^{1/3} F$ , (2) is transformed to a Bessel equation [12]

$$d^2F/dy^2 + y^{-1}dF/dy + (1 - 1/9y^2)F = 0 \quad (3)$$

The solution of (3) is a Bessel function of order 1/3, i.e.,  $F = J_{\pm 1/3}(y)$ , for  $y^2 > 0$ , or a modified Bessel function of the second kind of order 1/3, i.e.,  $F = K_{1/3}(|y|)$ , for  $y^2 < 0$ .

Therefore, the solutions of (2) in the two regions  $g > 0$  and  $g < 0$  are found to be

$$\text{and } \begin{cases} E_{\pm} = A_{\pm}g^{1/2}J_{\pm 1/3}((2/3)\sqrt{\nu}g^3) & \text{for } g > 0 \\ E = D|g|^{1/2}K_{1/3}((2/3)\sqrt{\nu}|g|^3) & \text{for } g < 0 \end{cases} \quad (4)$$

Applying the continuity condition to (4) at  $g = 0$ , i.e.,  $z = z_0$ , the solution of (2) in the region around  $z = z_0$  is obtained to be

$$E = \begin{cases} E_0g^{1/2}[J_{1/3}((2/3)\sqrt{\nu}g^3) + J_{-1/3}((2/3)\sqrt{\nu}g^3)] & \text{for } z \leq z_0 \\ E_+|g|^{1/2}K_{1/3}((2/3)\sqrt{\nu}|g|^3) & \text{for } z > z_0 \end{cases} \quad (5)$$

where  $E_+ = E_0[J_{1/3}(0) + J_{-1/3}(0)]/K_{1/3}(0)$ .

#### 4.2. A Specific Example of Wave Propagation in the Bottom-side of the Ionosphere

Let the turning point  $z_0 = 0$  to simplify the expression, so that  $g = -z$ . This field function  $E(x)$  is plotted in Fig. 5, where  $x = (2/3)\sqrt{\nu}z^3$ . As shown, the field amplitude near the turning point (i.e., the reflection height) is enhanced considerably by the cutoff effect. This is called the "swelling effect", which has a significant positive effect on exciting instabilities. Eq. (1) with a more realistic plasma density distribution can be solved by a finite element method [13].

### 5. NONLINEAR SCHROEDINGER EQUATION FOR LANGMUIR WAVES

Plasma waves are governed by a set of fluid equations, which, in essence, are nonlinear and coupled to each other. We will combine these equations into two; one describes the Langmuir wave, and the other the ion wave. They are coupled to each other due to the nonlinear nature of plasma. We will introduce some assumptions and make some

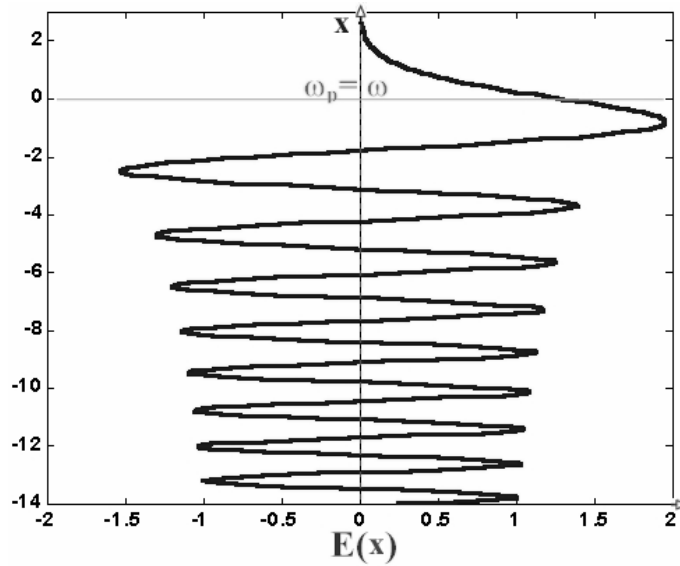


**Figure 5.** Distribution of the wave field near its turning point, where  $x = (2/3)\sqrt{\nu z^3}$ .

approximations. These two equations are then combined into a single one describing the nonlinear Langmuir waves.

### 5.1. Coupled Nonlinear Equation for the Langmuir Wave

The electron continuity and momentum equations, and divergence equation (Coulomb's law) are given by

$$\partial_t n_e + \nabla \cdot n_e \mathbf{v}_e = 0, \quad (6)$$

$$(\partial_t + \nu_e) n_e \mathbf{v}_e = -\nabla \cdot n_e \mathbf{v}_e \mathbf{v}_e - \nabla (P_e/m_e) - (e/m_e) n_e \mathbf{E}, \quad (7)$$

$$\nabla \cdot \mathbf{E} = -4\pi e (n_e - \hat{n}) = -4\pi e \delta n_e \quad (8)$$

where  $\partial_t = \partial/\partial t$ ;  $n_e = n_0 + \delta n_e + n_s$ ;  $\hat{n} = n_0 + n_s$ ;  $n_0$ ,  $\delta n_e$ , and  $n_s$  are the unperturbed plasma density and electron density perturbations associated with Langmuir waves and ion waves, respectively;  $\nu_e$  is the effective electron collision frequency;  $P_e$  is the electron pressure and the adiabatic relationship  $\nabla P_e = 3T_e \nabla \delta n_e$  will be used.

Apply the operation  $(\partial_t + \nu_e)$  to (6). With the aid of (7) and (8), a governing equation for the Langmuir wave field  $\mathbf{E}$  is derived to be

$$\left[ \partial_t (\partial_t + \nu_e) + \omega_p^2 - 3\nu_{te}^2 \nabla^2 \right] \mathbf{E} = -4\pi e \langle \nabla \cdot (n_e \mathbf{v}_e \mathbf{v}_e) \rangle - (\omega_p^2/n_0) (n_s \mathbf{E}) \quad (9)$$

where  $v_{te} = (T_e/m)^{1/2}$  is the electron thermal speed;  $\langle \nabla \cdot (n_e \mathbf{E}) \rangle = \nabla \cdot (n_s^* \varepsilon_p + n_0 \delta \mathbf{E}_L) = -4\pi e n_0 \delta n_e + \nabla \cdot (n_s \mathbf{E})$  is employed and  $\langle \rangle$  stands for a filter, which keeps only terms in the same frequency range.

This is a nonlinear mode equation of the Langmuir wave. The nonlinear nature of the equation is shown implicitly by the two terms on the RHS of (9). The second term on the RHS of (9) depends explicitly on the density perturbation of the ion wave and manifests the coupling between Langmuir waves and ion waves.

## 5.2. Coupled Nonlinear Equation for the Ion Wave

Both electrons and ions can effectively respond to low frequency wave fields. Hence, the formulation of the ion wave equation needs to include both electron and ion fluid equations. Since electrons and ions tend to move together, the formulation can be simplified by introducing the quasi-neutral condition:  $n_{si} \cong n_{se} = n_s$ . The ion fluid equations are similar to (6) and (7), except that the subscript  $e$  is changed to  $i$ , and the charge  $-e$  changed to  $e$ . Moreover, the collision terms  $v_e \mathbf{v}_e$  and  $v_i \mathbf{v}_i$  are replaced by  $v_e(\mathbf{v}_e - \mathbf{v}_i)$  and  $(m_e/m_i)v_e(\mathbf{v}_i - \mathbf{v}_e) + v_{in}\mathbf{v}_i$  in the electron and ion fluid equations, respectively, where  $v_e = v_{ei}$  is the electron-ion collision frequency and  $v_{in}$  is the ion-neutral particle collision frequency. When the quasi-neutral condition is applied to the continuity equations of the electron and ion fluids, one can show that  $|\mathbf{v}_{se}| \cong |\mathbf{v}_{si}|$ , i.e., electrons and ions tend to move together in the wave.

Combine the momentum equations of the electron (7) and the ion (analogy of (7)) fluids by adding them together. The electric field terms and electron-ion collision terms in the two equations cancel. Moreover, both the electron inertial term  $m_e \partial_t \mathbf{v}_e$  and the ion convective term  $m_i \mathbf{v}_i \cdot \nabla \mathbf{v}_i$  are small compared to their respective counterparts, and can be neglected. The result is

$$m_i(\partial_t + v_{in})\mathbf{v}_i + m_e \mathbf{v}_e \cdot \nabla \mathbf{v}_e = -n_0^{-1} \nabla(P_e + P_i) \quad (10)$$

With the aid of the quasi-neutrality, the relation  $\mathbf{v}_e \cdot \nabla \mathbf{v}_e = \nabla(v_e^2/2)$ , and the continuity equation  $\partial_t n_s + \nabla \cdot (n_0 \mathbf{v}_i) = 0$ , (10) becomes

$$[\partial_t(\partial_t + v_{in}) - C_S^2 \nabla^2](n_s/n_0) = (m_e/m_i) \nabla^2 \langle (v_e^2/2) \rangle \quad (11)$$

where the implicit nonlinear term on the RHS of (11) can be expressed explicitly in terms of the Langmuir wave field  $E$ .

## 5.3. Assumptions and Approximations

Consider only low frequency off-resonant ion waves, which are directly driven by the Langmuir waves. We can assume that  $|\partial_t(\partial_t +$

$v_{in})(n_s/n_0)| \ll |C_S^2 \nabla^2(n_s/n_0)|$  and (11) is approximated to obtain  $(n_s/n_0) \cong -(m_e/m_i) \langle (v_e^2/2) \rangle / C_S^2$ . Moreover, we will assume that  $|\langle (\nabla \cdot (n_e \mathbf{v}_e \mathbf{v}_e)) \rangle| \ll |(\omega_p^2/4\pi en_0) (n_s \mathbf{E})|$ . This assumption imposes an upper bound on the amplitude and a lower bound on the scale length of a nonlinear Langmuir wave governed validly by the equation in the formulation. Thus (9) reduces to

$$\left[ \partial_t(\partial_t + v_e) + \omega_p^2 - 3v_{te}^2 \nabla^2 \right] E = (\omega_{pi}^2/C_S^2) \langle (v_e^2/2) \rangle E \quad (12)$$

#### 5.4. Derivation of Nonlinear Schrodinger Equation for Langmuir Waves

Neglect the collision term on the LHS and the first two terms on the RHS of (7) and set  $E = \varepsilon(z, t) \exp[-i(\omega t - kz)] + \text{c.c.}$ , where  $\varepsilon(z, t)$  is the envelope of the wave,  $\omega = (\omega_p^2 + 3k^2 v_{te}^2)^{1/2}$  is the carrier frequency, and c.c. stands for complex conjugate. It leads to  $v_e \cong -i[e\varepsilon(z, t)/m_e \omega] \exp[-i(\omega t - kz)] + \text{c.c.}$ . Taking forward wave approximation, (12) reduces to

$$-2i\omega(\partial_t + v_g \partial_z)\varepsilon - 3v_{te}^2 \partial_z^2 \varepsilon - \left(\omega_{pi}^2/C_S^2\right) (e/m_e \omega)^2 |\varepsilon|^2 \varepsilon = 0 \quad (13)$$

Perform a coordinate transformation (to the moving frame with velocity  $v_g$ ) :  $t' = t$  and  $z' = z - v_g t$ , and reset  $(t', z')$  to  $(t, z)$  to simplify the presentation. Then (13) becomes

$$-(1/2m^*) \partial_z^2 \varepsilon - A|\varepsilon|^2 \varepsilon = i\partial_t \varepsilon \quad (14)$$

where  $m^* = \omega/3v_{te}^2$  and  $A = (\omega_{pi}^2/2\omega C_S^2)(e/m_e \omega)^2$ .

Eq. (14) is the nonlinear Schrodinger equation for the envelope of the Langmuir waves [14]. The second term on the LHS of (14) is a cubic nonlinear term and the operator of this term,  $-A|\varepsilon|^2$ , is the potential function of the Hamiltonian of the wave function  $\varepsilon$ . This potential function depends on the intensity of the wave, thus it is possible to trap the wave in a self-induced potential well. When this occurs, the wave will evolve into a localized nonlinear steady state called a ‘‘Soliton’’ as demonstrated below.

#### 5.5. Analysis

Substitute  $\varepsilon = e^{i\kappa z} F(\xi)$  into (14), where  $\xi = z - \kappa t$  and  $\kappa = m^* a$ , to obtain

$$F'' - \kappa^2 F + 2m^* A F^3 = 0 \quad (15)$$

where  $F'' = d^2F/d\xi^2$ . Multiply (15) by  $F'$ . The result can be integrated directly to obtain

$$F'^2 - \kappa^2 F^2 + m^* A F^4 = C \quad (16)$$

where the integration constant  $C$  is the equivalent energy of the wave. The solution of (16) is  $F' = \pm(C + \kappa^2 F^2 - m^* A F^4)^{1/2}$ , which becomes

$$dF/(C + \kappa^2 F^2 - m^* A F^4)^{1/2} = \pm d\xi \quad (17)$$

- 1)  $C > 0$ : (17) can be converted to the integral equation  $\int dF/(C + \kappa^2 F^2 - m^* A F^4)^{1/2} = \pm \xi$ ; this equation has periodic solutions.
- 2)  $C = 0$ : (16) becomes  $F'^2 - \kappa^2 F^2 + m^* A F^4 = 0$ ; this equation has a localized solution, which is given by

$$F = (\kappa^2/m^* A)^{1/2} \operatorname{sech} \kappa(z - at) = a(m^*/A)^{1/2} \operatorname{sech} \kappa(z - at)$$

This function (a “soliton”) and the self-induced potential well trapping this soliton are plotted in Fig. 6. The soliton is the result of the balance between the dispersion effect (represented by the first term on the LHS of (14)) and the nonlinearity (represented by the second term on the LHS of (14)) of the medium. The nonlinearity of the medium focuses the wave to overcome the wave dispersion in the propagation. Thus, a

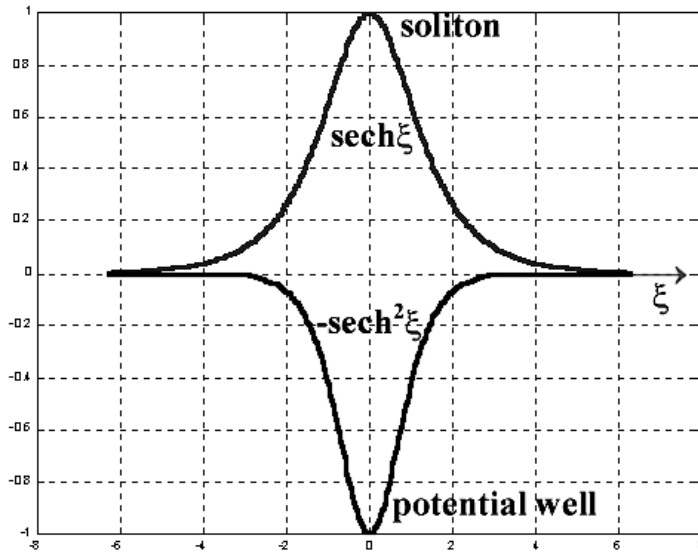


**Figure 6.** Soliton and its trapping potential well.

shape-preserved soliton can exist. Under different physical situations, the nonlinearity may change. A localized solution still exists as long as the balance between the dispersion effect and the nonlinearity of the medium can be achieved [15]. However, it should be noted that this localized solution exists only under the condition  $C = 0$ , i.e., only if the initial source wave is localized. Otherwise, the solution of the nonlinear Schrodinger equation is a periodic function. In other words, plasma can support Langmuir solitons, but Langmuir soliton is not a necessity of the plasma nonlinearity; the solution of the nonlinear Schrodinger equation is either a periodic function or a soliton, depending on the initial/boundary conditions of the source wave function.

In heating experiments, the heating wave covers a large cross sectional area (a few tens of km in diameter). Therefore, under the normal conditions, it is not likely to excite the localized Langmuir waves as the source waves, which would evolve nonlinearly into Langmuir solitons.

#### ACKNOWLEDGMENT

I am grateful to Paul Kossey, Lee Snyder, Edward Kennedy, M. C. Lee, and Leo Birenbaum for helpful discussions. This work was supported by the High Frequency Active Auroral Research Program (HAARP), the Air Force Research Laboratory at Hanscom Air Force Base, MA, and by the Office of Naval Research Grant ONR-N00014-05-1-0109. Part of the financial support of this work was provided by a subcontract from NorthWest Research Associates, Inc.

#### REFERENCES

1. Gordon, W. E. and H. C. Carlson, "Arecibo heating experiments," *Radio Sci.*, Vol. 9, 1041, 1974.
2. Hagfors, T., W. Kofman, H. Kopka, P. Stubbe, and T. Aijanen, "Observations of enhanced plasma lines by EISCAT during heating experiments," *Radio Sci.*, Vol. 18, 861, 1983.
3. Stubbe, P., H. Kohl, and M. T. Rietveld, "Langmuir turbulence and ionospheric modification," *J. Geophys. Res.*, Vol. 97, 6285, 1992.
4. Fejer, J. A., "Ionospheric modification and parametric instabilities," *Rev. Geophys.*, Vol. 17, 135, 1979.
5. Kossey, P., J. Heckscher, H. Carlson, and E. Kennedy, "HAARP: High frequency active auroral research program," *Journal of*

- Arctic Research of the United States*, Vol. 1, Spring/Summer, 1999.
6. Stubbe, P., H. Kopka, and R. L. Downen, "Generation of ELF and VLF waves by polar electrojet modulation: experimental results," *J. Geophys. Res.*, Vol. 86, 9073, 1981.
  7. Mphale, K. and M. Heron, "Ray tracing radio waves in wildfire environments," *Progress In Electromagnetics Research*, PIER 67, 153–172, 2007.
  8. Perkins, F. W., C. Oberman, and E. J. Valeo, "Parametric instabilities and ionospheric modification," *J. Geophys. Res.*, Vol. 79, 1478, 1974.
  9. Kuo, S. P., "Oscillating two stream instability in ionospheric heating experiments," *Phys. Plasmas*, Vol. 9, 1456, 2002.
  10. Kuo, S. P., "Cascade of the parametric decay instability in ionospheric heating experiments," *J. Geophys. Res.*, Vol. 106, 5593, 2001.
  11. Kuo, S. P. and M. C. Lee, "Cascade spectrum of HFPLs generated in HF heating experiments," *J. Geophys. Res.*, Vol. 110, A01309, 2005; doi:10.1029/2004JA010674.
  12. Ginzburg, V. L., *The Propagation of Electromagnetic Waves in Plasmas*, 2nd edition, Pergamon, New York, 1970,
  13. Isaakidis, S. A. and T. D. Xenos, "Wave propagation and reflection in the ionosphere. An alternative approach for ray path calculations," *Progress In Electromagnetics Research*, PIER 45, 201–215, 2004.
  14. Schmidt, G., *Physics of High Temperature Plasmas*, 2nd edition, Chapter 9, 304–318, Academic Press, 1979.
  15. Konar, S. and A. Biswas, "Soliton-soliton interaction with power law nonlinearity," *Progress In Electromagnetics Research*, PIER 54, 95–108, 2005.